Biosensors and Bioelectronics 102 (2018) 94–100

Contents lists available at ScienceDirect

Biosensors and Bioelectronics

journal homepage: www.elsevier.com/locate/bios

Cerium dioxide-doped carboxyl fullerene as novel nanoprobe and catalyst in electrochemical biosensor for amperometric detection of the *CYP2C19*2* allele in human serum

Chengli Zhang[1], Junlin He[1], Yuchan Zhang, Jun Chen, Yilin Zhao, Yazhen Niu, Chao Yu*

College of Pharmacy, Institute of Life Science and School of Public Health, Chongqing Medical University, Chongqing 400016, PR China

ARTICLE INFO

Keywords:
Clopidogrel
*CYP2C19*2* gene
Cerium dioxide nanoparticles
Metal-organic frameworks
Electrochemical DNA sensor

ABSTRACT

The disposition dose of clopidogrel is different in *CYP2C19*2* gene carriers and non-carriers. High-dose clopidogrel has been recommended to overcome a low-responsiveness to clopidogrel in patients with the *CYP2C19*2* gene. To guide the choice of clopidogrel dosage and catalyse a development in the field of personalized therapy, we developed an ultrasensitive electrochemical biosensor to detect *CYP2C19*2* gene. We constructed a novel assay based on cerium dioxide (CeO_2)-functionalized carboxyl fullerene (c-C_{60}) supported by Pt nanoparticles (c-C_{60}/CeO_2/PtNPs) for signal amplification. Au nanoparticles @ Fe-MIL-88NH_2 (AuNPs@Fe-MOFs) were synthesized by one-step method as the support platform to enhance the conductivity and immobilize more biotin-modified capture probe (bio-CP) through the superior affinity and specificity between streptavidin and biotin. c-C_{60}/CeO_2/PtNPs were labeled with signal probe to form the signal label. After the sandwich reaction of *CYP2C19*2* gene between capture probe and the signal label, a distinguishing electrochemical signal from the catalysis of H_2O_2 by signal label would be observed. Amperometry was applied to record electrochemical signals. Under optimized conditions, the approach showed a good linear dependence between current and the logarithm of *CYP2C19*2* gene concentrations in the range of 1 fM to 50 nM with a low detection limit of 0.33 fM (S/N = 3). The proposed method showed good specificity to target DNA compared with possible interfering substances. More importantly, the fabricated biosensor achieved accurate quantitative detection of *CYP2C19*2* gene in human serum samples demonstrated by excellent correlations with standard DNA sequencing and provided a promising strategy for electrochemical biosensor detection of other gene mutations.

1. Introduction

Clopidogrel inhibits adenosine diphosphate-induced platelet aggregation and has been shown to reduce cardiovascular events in patients with acute coronary syndrome, especially in those undergoing percutaneous coronary intervention (Hamm et al., 2011; Levine et al., 2013). However, there is a large degree of difference among individuals in the pharmacodynamic response to clopidogrel (Angiolillo et al., 2007). The CYP2C19 protein is required for the conversion of clopidogrel to its active metabolite (thiol metabolite). However, the presence of defective alleles of the *CYP2C19* has been associated with lower levels of the active metabolite corresponding in turn to diminished antiplatelet effect and potentially higher rates of adverse cardiovascular events (Campo et al., 2010). The *CYP2C19*2* and *CYP2C19*3* gene are associated with reduced levels of clopidogrel's active metabolite. Especially, the *CYP2C19*2* gene carriers have lower active metabolite levels of clopidogrel and were reported as the major *CYP2C19* variant found in Chinese (Hu et al., 2012; Hulot et al., 2006; Li et al., 2014; Luo et al., 2006). In addition, accumulated evidence supports the relationship between *CYP2C19 *2* gene and high on-treatment platelet reactivity (HTPR) and the risk of ischaemic cardiovascular event in clopidogrel-treated patient (Bauer et al., 2011; Holmes et al., 2011; Mega et al., 2010). Thus, the detection of *CYP2C19*2* gene provides worthy insight into early clinical treatment and response monitoring (Wei et al., 2010). Moreover, personalized therapy is needed to effectively detect the genotype of *CYP2C19*2*, which can contribute to pharmacological treatments.

Conventional techniques for *CYP2C19*2* gene detection have been reported, such as DNA sequencing (Tang et al., 2016), real-time quantitative polymerase chain reaction (qPCR) (Koukoula et al., 2017) and restriction fragment length polymorphism analysis (PCR-RFLP) (De Morais et al., 1994). However, these methods are time-consuming, have

* Corresponding author.
E-mail address: yuchaom@163.com (C. Yu).
[1] Junlin He and Chengli Zhang contributed equally to this work.

http://dx.doi.org/10.1016/j.bios.2017.11.014
Received 24 August 2017; Received in revised form 10 October 2017; Accepted 1 November 2017

a high cost and require high-precision equipment. Thus, exploring an effective, simple, and highly sensitive testing for *CYP2C19*2* gene appears to be a realistic goal.

Electrochemical biosensors have received attention because of their low cost, simplicity, minimal sample preparation, sensitivity and short response time (Li et al., 2016). To achieve the high sensitivity of a "sandwich" type biosensor, an important component needs to be improved: "the recognition layer" (Zeng et al., 2015). Metal-organic frameworks (MOFs) are a relatively new class of porous inorganic-organic materials with fascinating structures and intriguing properties, such as high specific surface areas, tunable pore sizes and exposed active sites, good thermal stability and uniform structured nanoscale cavities (Yu and Yan, 2013). In addition, the Fe-MIL-88NH_2(Fe-MOFs) not only inherited the above advantages but also exhibited high stability and good biocompatibility in aqueous solution (Liu et al., 2013). Thus, Fe-MOFs have drawn a high degree of attention as a template. To improve the sensitivity of the proposed biosensor and capture more streptavidin (SA), gold nanoparticles (AuNPs) were introduced to immobilize SA via Au-NH_2 bonds. Herein, Fe-MOFs were used as the template to immobilize AuNPs and obtained the AuNPs@Fe-MOFs compounds. Compared with individual AuNPs, AuNPs@Fe-MOFs confer much higher selectivity and sensitivity to biosensor.

Meanwhile, "the signal transducer layer" was the other key component that needed to be improved (Zeng et al., 2015). Nanocomposites with excellent catalytic properties can greatly improve the sensitivity of detection. Cerium dioxide (CeO_2) nanoparticles have attained significant attention due to their unique catalysis properties, high adsorption capability and enhancement of the electrons transfer effect between the electrode and materials modified on the electrode surface (Li et al., 2017). Due to the above advantages, there have been extensive applications in the field of catalysis in the form of pure CeO_2 or immobilization of metal components (Zhang et al., 2012). However, the prepared CeO_2 usually forms aggregates that lead to a lower catalytic activity. To improve the stability of CeO_2, carboxyl fullerene (c-C_{60}) was introduced for its high stability and large surface area. In addition, c-C_{60} shows better water dispersibility compared with fullerene. Thus, a simpler synthesis method and the application of non-toxic solvents have been achieved in the synthesis of c-C_{60}/CeO_2/PtNPs. Finally, c-C_{60} with large specific area can bind with more CeO_2 nanoparticles to amplify the signal (Chen et al., 2016; Lu et al., 2014; Yu et al., 2016). Moreover, to bring the role of CeO_2 into full play for signal amplification, platinum nanoparticles (PtNPs) were chosen, binding with the signal probe, owing to its significantly electrocatalytic activity, adsorbing strongly to amino and thiol groups (Zhang et al., 2014). The synergistic catalysis of CeO_2/PtNPs achieves the signal amplification by catalysing H_2O_2. In summary, compared with individual CeO2 and PtNPs, c-C60/CeO2/PtNPs composites have more efficient catalytic ability because of the synergistic catalysis of H2O2 by CeO2 and PtNPs and the large surface area of c-C_{60}. Thus, the combination of c-C_{60}, CeO_2 and PtNPs achieved signal amplification.

Here, we report an ultrasensitive DNA biosensor for the specific detection of the *CYP2C19*2* gene mutation using AuNPs@Fe-MOFs as the support platform and c-C_{60}/CeO_2/PtNPs composites as signal amplification tag. AuNPs@Fe-MOFs, c-C_{60}/CeO_2/PtNPs and the biotin-streptavidin system in this study have the following four major advantages: (1) AuNPs@Fe-MOFs have remarkable conductivity and bigger contact areas with biomolecules as one Fe-MOF particle can support many AuNPs on its surface, which loaded more SA and enhanced the sensitivity of our sensor. (2) The biotin-SA system improves the sensitivity of the proposed DNA sensor because one SA molecule can bind four biotin molecules. (3) Compared with individual CeO_2 and PtNPs, c-C_{60}/CeO_2/PtNPs composites have more efficient catalytic ability because of the syncatalysis of H_2O_2 by CeO_2 and PtNPs. (4) The use of the water-soluble substance c-C_{60} simplifies the synthesis of the c-C_{60}/CeO_2/PtNPs. Hence, the synthesis method possesses greater practicality, repeatability and non-toxic solvent. Finally, 20 clinical samples were detected and compared with the sequencing method. The proposed electrochemical DNA sensor showed ultrasensitivity, precision, good stability, and reproducibility, suggesting a wide range of potential diagnostic applications to detect low amounts of *CYP2C19*2* gene.

2. Experimental

2.1. Reagent and apparatus

The reagents and apparatus are described in detail in the Supplementary information (S1-S2).

2.2. Preparation of Fe-MIL-88 MOFs and AuNPs@Fe-MIL-88-MOFs

Fe-MIL-88 MOFs were synthesized according to the literature (Liu et al., 2013). AuNPs@Fe-MOFs were prepared by the $NaBH_4$ reduction method. Briefly, 0.126 g of 2-aminoterephthalic acid and 0.187 g of $FeCl_3{\cdot}6H_2O$ were dissolved in 15 mL of dimethylformamide (DMF). The mixture was kept in a silicone oil bath at 120 °C for 4 h under continuous magnetic stirring. After reacting for 15 min, 3.45 mM acetic acid was added to this solution. After slowly cooling to 25 °C, the prepared Fe-MOFs were purified by centrifugation and washed with DMF, ethanol and ultrapure water to remove surplus reactants. Finally, the precipitate was dried in a vacuum oven overnight. The synthesis of AuNPs@Fe-MOFs was as follows: First, 1 mL of $HAuCl_4{\cdot}4H_2O$ (1.0%, w/v) was added to 1 mL of the prepared Fe-MOFs solution (1 mg mL^{-1}) and vigorously sonicated for 15 min. Subsequently, 2 mL of a $NaBH_4$ solution (3.8 mg mL^{-1}) was dropwise added to the mixture with stirring for 30 min. Then, the mixture was purified by centrifugation and washed with Milli-Q water three times. Finally, the prepared products were dried at 50 °C for 12 h before use.

2.3. Preparation of c-C_{60}/CeO_2

Previously method was used for the preparation of c-C_{60}/CeO_2 composites with a little modification (Ujjain et al., 2014). First, 10 mg of c-C_{60} was dissolved in 5 mL of ultrapure water under ultrasonication for 10 min at room temperature. Next, 10 mL of $Ce(NO_3)_3{\cdot}6H_2O$ (10.8 mg mL^{-1}) was mixed with 10 mL of hexamethylenetetramine (3.5 mg mL^{-1}). Then, both solutions were mixed and kept in a water bath at 80 °C for 5 h and washed with Milli-Q water several times. Subsequently, the prepared precipitate was dried at 60 °C before further use.

Subsequently, 20 mg of c-C_{60}/CeO_2 composites were dispersed in 5 mL of ethanol and sonicated for 15 min to obtain dispersive solution. Then, 0.1 mL of 3-aminopropyltriethoxysilane (98%) was mixed with the above solution and kept reflux at 70 °C for 1.5 h. After cooling to room temperature, the obtained c-C_{60}/CeO_2 composites were washed with ultrapure water by centrifugation at 8000 rpm. Eventually, the prepared products were dried at 50 °C before further use.

2.4. Preparation of c-C_{60}/CeO_2/PtNPs, PtNPs, c-C_{60}/PtNPs and c-C_{60}/CeO_2/AuNPs

The PtNPs supported on c-C_{60}/CeO_2 were synthesized by the $NaBH_4$ reduction method. Briefly, 1 mL of $H_2PtCl_6{\cdot}6H_2O$ (1.0%, w/v) was added to 1 mL of c-C_{60}/CeO_2 solution (2 mg mL^{-1}) and vigorously sonicated for 5 min. Then, 2 mL of a $NaBH_4$ solution (3.8 mg mL^{-1})was added dropwise to the mixture with stirring for 30 min, followed by centrifuging, washing with Milli-Q water, and dissolving in 1 mL of Milli-Q water for further use. c-C_{60}/CeO_2/AuNPs and c-C_{60}/PtNPs composites were synthesized by a similar method, except that 1 mL of H_2PtCl_6 (1%) was displaced by 1 mL of $HAuCl_4{\cdot}4H_2O$ (1.0%, w/v) and 1 mL of c-C_{60}/CeO_2 (2 mg mL^{-1}) was displaced by 1 mL of c-C_{60} (2 mg mL^{-1}). PtNPs were prepared as follows. First, 1 mL of

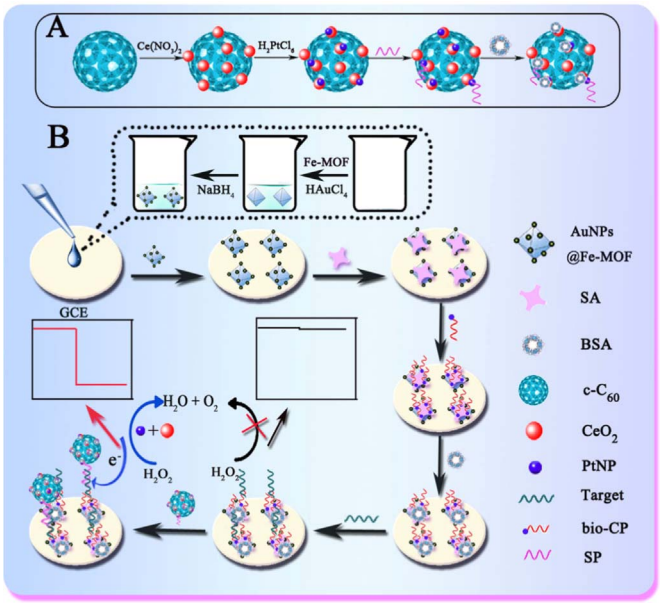

Scheme 1. (A) The preparation process of the c-C_{60}/CeO_2/PtNPs/SP signal probes. (B) Schematic illustration of the assembly procedure of the electrochemical biosensor.

$H_2PtCl_6.6H_2O$ (1.0%, w/v) was added to 1 mL of Milli-Q water. Then, 2 mL of $NaBH_4$ solution (3.8 mg mL^{-1})was added dropwise into the above solution with stirring for 30 min, followed by centrifuging and washing with Milli-Q water. The synthesized products were dissolved in 1 mL of Milli-Q water.

2.5. Preparation of c-C_{60}/CeO_2/PtNPs/SP, c-C_{60}/CeO_2/AuNPs/SP, c-C_{60}/PtNPs/SP and PtNPs/SP

In brief, 1 mL of as-prepared c-C_{60}/CeO_2/PtNPs were mixed with 200 μL of 1 μM amino-modified signal probe (SP) and stirred gently at 4 °C for 24 h. Afterward, 1 mg of BSA was added to 1 mL of TE buffer and the mixture was used to block the nonspecific binding sites of c-C_{60}/CeO_2/PtNPs for another 4 h. Then, c-C_{60}/CeO_2/PtNPs/SP/BSA bioconjugates were centrifuged at 8000 rpm and washed three times with Milli-Q water, followed by dispersal in 1 mL of hybridization solution for further use. The preparation process of c-C_{60}/CeO_2/PtNPs/SP is shown in Scheme 1A. The c-C_{60}/CeO_2/AuNPs/SP were synthesized by a similar method, except that c-C_{60}/CeO_2/PtNPs were displaced by c-C_{60}/CeO_2/AuNPs. Furthermore, c-C_{60}/PtNPs/SP and PtNPs/SP bioconjugates were also synthesized with an analogous process for c-C_{60}/CeO_2/PtNPs/SP, except that c-C_{60}/CeO_2/PtNPs were displaced by c-C_{60}/PtNPs and PtNPs.

2.6. Fabrication of the sensing interfaces

Scheme 1 shows the preparation procedure of the biosensor. Prior to modification, GCE was successively polished with 0.3 and 0.05 μm alumina powders, and the electrode was then sequentially sonicated in Milli-Q water, alcohol and Milli-Q water for 5 min. Initially, 6 μL of AuNPs@Fe-MOFs aqueous suspension (2 mg mL^{-1}) was cast onto the electrode surface. After drying, 10 μL of SA (100 μg mL^{-1}) solution was coated onto the AuNPs@Fe-MOFs nanocomposite-modified electrode for 12 h at 4 °C. After that, these electrodes were washed with Milli-Q water to remove unbound SA and dried in air. Then, 10 μL of 1 μM bio-CP was cast onto the GCE/AuNPs@Fe-MOFs and incubated at 4 °C for 12 h. Then, the modified electrode was rinsed with washing buffer and placed into 6 μL of BSA (1%, w/v) for 30 min at 37 °C to eliminate nonspecific adsorption.

2.7. Electrochemical measurements

Detection was based on the typical procedures of the sandwich reaction (Dong et al., 2012). The DNA biosensor (GCE/AuNPs@Fe-MOFs/SA/bio-CP/BSA) was incubated with various concentrations of target DNA for 2 h at 37 °C. The obtained c-C_{60}/CeO_2/PtNPs/SP was coated on GCE/AuNPs@Fe-MOFs/SA/bio-CP/BSA/target electrode for 2 h at 37 °C. After the reaction, the electrode was washed with washing buffer to remove unbound conjugates. Ultimately, the electrochemical signal of the amperometric i-t curve was recorded at 0.4 V in 5 mL of phosphate buffered saline (PBS). When the background current was stable, 20 μL of H_2O_2 (1.4 mol L^{-1}) was added to the PBS solution, and then the current changes were recorded. Current0 is the blank specimen current change and Current is the specimen current change: ΔCurrent = Current - Current0.

3. Results and discussion

3.1. Characteristics of the AuNPs@Fe-MOFs composites

FE-SEM was used to characterize the size and morphology of the as-prepared nanomaterials. As shown in Fig. S1A, most of the Fe-MOFs had a regular octahedron structure. The average diameter of Fe-MOFs was approximately 200 nm, which was in accordance with the previous report (Liu et al., 2013). After AuNPs were in situ reduced on the surface of Fe-MOFs, a large number of bright dots spread along the Fe-MOFs were observed, as distinguished from Fe-MOFs, as shown in Fig. S1B. A further demonstration of the formation of the AuNPs@Fe-MOFs composites by EDS and ζ-potential were displayed. As shown in Fig. S1C, there were significant peaks corresponding to C, N, O, Au and Fe in the EDS image of AuNPs@Fe-MOFs. The ζ-potential of Fe-MOFs and AuNPs@Fe-MOFs were 20.5 and 15.3, respectively (Fig. S1D). These results further indicated the successful modification of Fe-MOFs by the negatively charged AuNPs (Wang et al., 2017). These results revealed that AuNPs@Fe-MOFs were successfully synthesized.

3.2. Characterization of the c-C_{60}/CeO_2/PtNPs composites

To verify the successful formation of the signal materials, FE-SEM and EDS were used. As shown in Fig. 1A, the c-C_{60} showed a typically spherical shape and the average size of c-C_{60} was approximately 100 nm. Fig. 1B shows the typical structure of CeO_2 with an average diameter of approximately 20 nm, which was in accordance with previous reports (Ujjain et al., 2014). As shown in Fig. 1C, the as-obtained CeO_2 were dispersed on the surface of c-C_{60}, the average diameter of the hybrid was approximately 150 nm. Meanwhile, there were significant peaks corresponding to C, O and Ce in the EDS image of c-C_{60}/CeO_2 (Fig. 1E). From these results, it was confirmed that the c-C_{60}/CeO_2 had been successfully synthesized. After PtNPs were in situ reduced on the surface of c-C_{60}/CeO_2, a large number of bright dots spread along the c-C_{60}/CeO_2 were observed (Fig. 1D). EDS characterization of c-C_{60}/CeO_2/PtNPs was also employed. As shown in Fig. 1F, several intense peaks of Pt were observed, suggesting that PtNPs were successfully modified on c-C_{60}/CeO_2, proving the successful synthesis of c-C_{60}/CeO_2/PtNPs. X-ray photoelectron spectroscopy (XPS) was used to further confirm the successful synthesis of c-C_{60}/CeO_2/PtNPs composites. As showed in Fig. 1G, the characteristic peaks for the Pt4f, C1s, O1s and Ce3d core level regions were clearly observed in the c-C_{60}/CeO_2/PtNPs composites. The composites showed the spectrum of C1s, O1s and Ce3d, verifying the successful synthesis of c-C_{60}/CeO_2. Moreover, the Pt4f core level suggested that the c-C_{60}/CeO_2 effectively anchored PtNPs. The spectrum of Ce3d and Pt4f are displayed in Fig. 1H and I. These results revealed that c-C_{60}/CeO_2/PtNPs composites were successfully synthesized (Deng et al., 2014). In addition, a further testimony of the formation of the c-C_{60}/CeO_2/PtNPs through ζ-potential and FT-IR spectroscopy were displayed in S3.1.

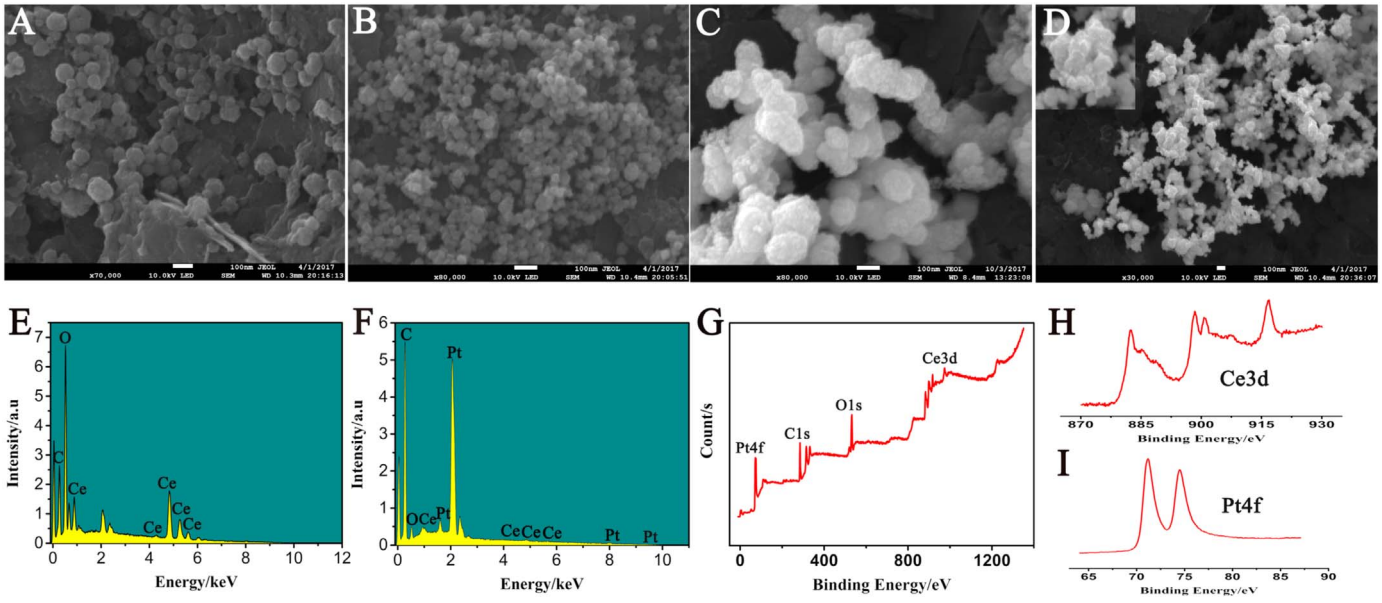

Fig. 1. FE-SEM images of (A) c-C_{60}, (B) CeO_2, (C) c-C_{60}/CeO_2 and (D) c-C_{60}/CeO_2/PtNPs composite. EDS of (E) c-C_{60}/CeO_2 and (F) c-C_{60}/CeO_2/PtNPs composite. (G) The XPS spectrum of c-C_{60}/CeO_2/PtNPs. The spectra of Ce3d in c-C_{60}/CeO_2/PtNPs (H) and Pt4f in c-C_{60}/CeO_2/PtNPs(I).

Specific coupling among the target DNA, bio-CP and SP were investigated by agarose gel electrophoresis. In Fig. S3, lane a was 20 bp marker and bio-CP (lane b) exhibited the highest mobility due to its low molecular weight. The bio-CP-target DNA conjugates (lane d) showed lower mobility, compared with target DNA (lane c) and bio-CP. The above results verified the successful hybridization of bio-CP and target DNA. Further, compared with SP (lane e), lane f had the same volume of bio-CP and SP added and had no significant mobility change. However, the band intensity was weakened because SP cannot hybridize with bio-CP. To verify the successful hybridization of SP and target DNA, lane g revealed that SP can hybridize with the target and have a lower mobility than lane e. Finally, after target DNA was hybridized with SP and bio-CP, lane h showed the lowest mobility, which confirmed that target DNA successfully hybridized with bio-CP and SP. These results testified the hybridization feasibility of our DNA biosensor.

3.3. The electrochemical behaviour of different nanomaterials for signal tags

The electrochemical behaviours of different nanomaterials were compared by amperometric i-t curves. As shown in Fig. 2A, curve a showed the i-t responses of c-C_{60}, which verified c-C_{60} has no catalytic ability with H_2O_2. Compared with curve a, the current of curve b was increased. Thus, CeO_2 (curve b) showed certain catalytic ability. This result indicated that CeO_2 can catalyse H_2O_2, which is consistent with previous report (Ujjain et al., 2014). After CeO_2 was linked with c-C_{60}, the composite of c-C_{60}/CeO_2 (curve c) showed an enhanced catalysis ability compared with curves a and b owing to the large specific area of c-C_{60}, which can increase the loading of CeO_2 and enhance the catalytic ability. The inset showed enlarged details of curves a, b and c. Finally, when PtNPs were assembled on the surface of CeO_2, the current value was distinctly increased (curve e) due to the syncatalytic effect of CeO_2 and PtNPs. Moreover, curves d showed the electrochemical response of c-C_{60}/CeO_2/AuNPs, which indicated that PtNPs exhibited better catalytic ability than AuNPs. These results demonstrated that the proposed signal material used in this biosensor has the best catalytic ability compared with the other materials in this experiment.

3.4. Electrochemical characterization of the stepwise modified electrodes

The stepwise fabrication process of the biosensor was electrochemically characterized by CV and electrochemical impedance spectroscopy (EIS) in a 5 mM $[Fe(CN)_6]^{3-/4-}$ solution. The results of CV were shown in Fig. 2B, the curve of the bare GCE (curve a) had a pair of typical reversible redox peaks. After the AuNPs@Fe-MOFs were coated onto the electrode, the peak current was obviously increased (curve b), because of the excellent electrical conductivity of AuNPs@Fe-MOFs. After SA was coated on the modified electrode, the peak current was decreased (curve c) owing to the poor conductivity of SA. When bio-CP was added, the peak current was further decreased (curve d) because of the negatively charged phosphate backbone of the capture probe could prevent the ferricyanide anions from approaching the electrode surface. After blocking with BSA, a further decrease was observed on the peak current (curve e), due to the non-conductivity of BSA hindering electron transfer.

As shown in Fig. 2C, EIS was used to further verify the stepwise-modified processes of the proposed electrode in a 5 mM $[Fe(CN)_6]^{3-/4-}$ solution. The diameter of the semicircle in EIS was related to charge transfer resistance (R_{et}). The inset was the equivalent circuit used to fit the impedance spectra. C_{dl} represented the double layer capacitance, R_S represented the electrolyte resistance and Z_W represented the Warburg impedance. The bare GCE presented a small semicircle (curve a) with a R_{et} value of 389.2 Ω. When the AuNPs@Fe-MOFs were coated onto the electrode, the resistance decreased to 149.2 Ω (curve b) because AuNPs@Fe-MOFs promote the electron transfer of the electrode. After SA was coated on the modified electrode, the diameter of the semicircle was increased (curve c, 388.7 Ω), indicating that non-conductive SA was successfully immobilized onto the electrode. Then, the resistance increased remarkably (curve d, 576.7 Ω) after the electrode was incubated with the bio-CP due to negatively charged phosphate backbone of the capture probe preventing the ferricyanide anions from approaching the electrode surface. Subsequently, a larger semicircular diameter was observed when the electrode was blocked with BSA (curve e, 722.9 Ω) because of the formation of a hydrophobic protein layer. The results of EIS were consistent with the CVs. Moreover, the fabrication process was also investigated by atomic force microscopy (see details in Supplementary information). These data suggested the successful fabrication of the biosensor.

3.5. The feasibility of signal-amplifcation strategies

To investigate the signal amplification of the proposed biosensor,

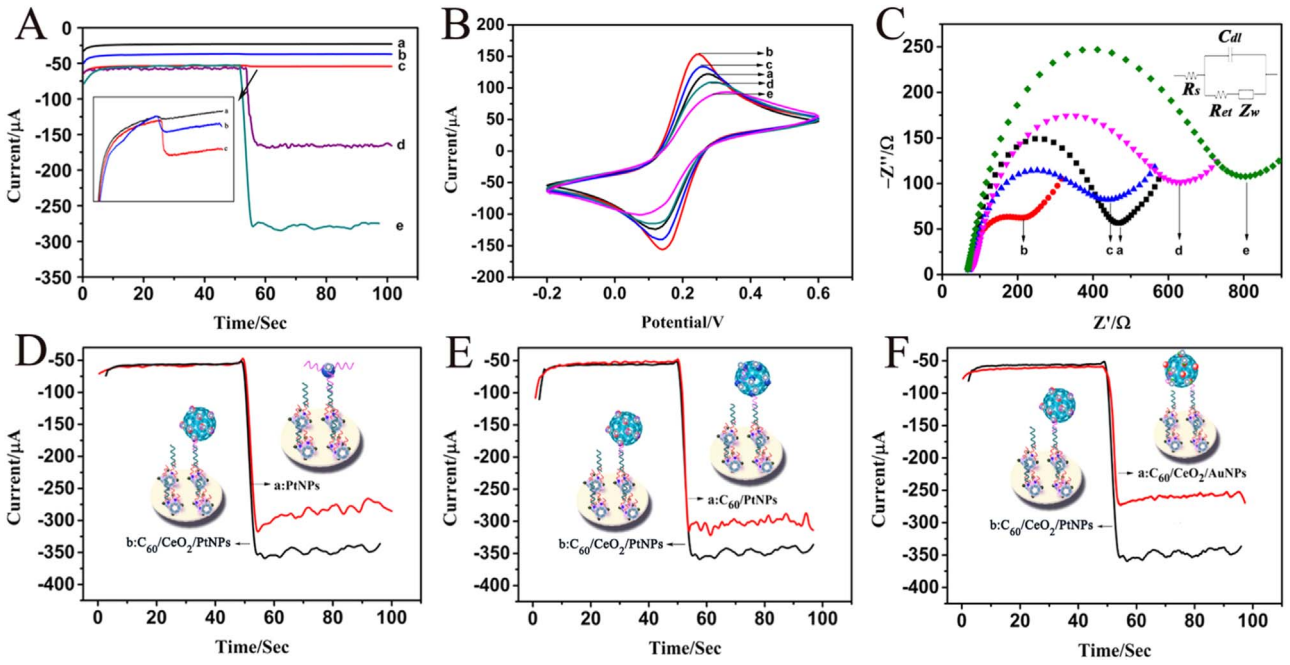

Fig. 2. (A) The amperometric i-t curves of different nanomaterials: (a) c-C_{60}, (b) CeO_2, (c) c-C_{60}/CeO_2, (d) c-C_{60}/CeO_2/AuNPs, and (e) c-C_{60}/CeO_2/PtNPs. (B) CV and (C) EIS characterization of electrodes at various stages of modification in a 5 mM $[Fe(CN)6]^{3-/4-}$ solution: (a) bare GCE, (b) GCE/AuNPs@Fe-MOFs, (c) GCE/AuNPs@Fe-MOFs/SA, (d) GCE/AuNPs@Fe-MOFs/SA/bio-CP and (e) GCE/AuNPs@Fe-MOFs/SA/bio-CP/BSA. Amperometric i-t curves of different nanomaterials after the format bioreaction of the proposed biosensor in the presence of 100 p.M. target DNA: (D) catalysis of PtNPs/SP and c-C_{60}/CeO_2/PtNPs/SP. (E) catalysis of c-C_{60}/PtNPs/SP and c-C_{60}/CeO_2/PtNPs/SP. (F) catalysis of c-C_{60}/CeO_2/AuNPs/SP and c-C_{60}/CeO_2/PtNPs/SP.

the biosensor was utilized with three types (PtNPs/SP, c-C_{60}/PtNPs/SP, and c-C_{60}/CeO_2/AuNPs/SP) of labeled probes with the same concentration (100 pM) of target DNA (Fig. 2). As shown in Fig. 2D, the current response of the biosensor with c-C_{60}/CeO_2/PtNPs/SP was improved in comparison with that of PtNPs/SP. This improvement owes to the catalytic activity of CeO_2 and PtNPs towards H_2O_2. Additionally, when the biosensor was incubated with c-C_{60}/PtNPs/SP (Fig. 2E), the current response was increased compared with that of PtNPs/SP. c-C_{60} has a large surface area, which makes it a great nanocarrier and increased the loading amounts of PtNPs (Chen et al., 2016). Compared with c-C_{60}/CeO_2/PtNPs/SP, the current response of c-C_{60}/PtNPs/SP (Fig. 2E) was lower. These results were attributed to the syncatalytic activity of CeO_2 and PtNPs towards H_2O_2 and indicated that the c-C_{60}/CeO_2/PtNPs nanomaterial enhanced the catalytic ability towards H_2O_2. Moreover, the current response was remarkably increased when the biosensor was incubated with c-C_{60}/CeO_2/PtNPs/SP compared with the c-C_{60}/CeO_2/AuNPs/SP (Fig. 2F) because the catalytic ability of PtNP is stronger than that of AuNP (Liu et al., 2014). Thus, we chose c-C_{60}/CeO_2/PtNPs/SP as the signal tag throughout the experiment.

3.6. Optimization of the experimental conditions

The optimum conditions (the volume of AuNPs@Fe-MOFs, the concentration of SA, the immobilization time of bio-CP, incubation time, and the concentration of H_2O_2 and pH of the testing solution) were determined as shown in Fig. S5. The detailed descriptions are shown in the Supplementary information.

3.7. Analytical performance of the biosensor

Under optimal experimental conditions, the proposed biosensor was incubated with a series of concentrations of target DNA, and the amperometric i-t curve was recorded by adding 20 μL of H_2O_2 to PBS every 50 s. As shown in Fig. 3A, the current changes increased with the increment of the target DNA (*CYP2C19*2* gene) from 1 fM to 50 nM. Fig. 3B shows a linear dependence between current and the logarithm of *CYP2C19*2* gene concentrations. The linear regression equation was $Y = 44.60 + 33.53*X$ ($R^2 = 0.9980$). The detection limit was estimated to be 0.33 fM (based on S/N = 3). This biosensor has been compared with the other sensor for *CYP2C19*2* gene mutation determination and listed in Table S4. The prepared biosensor exhibited a low detection limit. The low detection limits might be due to the excellent conductivity of AuNPs@Fe-MOFs, the signal amplification of the biotin-streptavidin system and the remarkably catalytic ability of c-C_{60}/CeO_2/PtNPs towards H_2O_2. To better show the advantages of this DNA sensor, the associated performance parameters (e.g., detection limit, linear range) have been compared with those obtained by other similar strategies and listed in Table S5.

3.8. Specificity, reproducibility, and stability of proposed biosensor

To evaluate the specificity of the developed biosensor, some different concentration targets, target mixtures and nonspecific interference DNA, including target DNA (5 fM, 100 fM, 100 pM, 50 nM), single-base mismatched DNA (SBM), double-base mismatched DNA (DBM), three-base mismatched DNA (TBM), non-complementary DNA (NC), blank controls and target mixtures were tested, and the results are shown in Fig. 3C and D. As could be seen, with an excess amount of nonspecific interference DNA, the prepared biosensor showed negligible interference to the above mismatched DNA sequences. The amperometric i-t curve current response variation due to the interfering substances was less than 5% of that without interferences. These results indicated the high specificity of the biosensor to its complementary target DNA. To evaluate the stability of the DNA sensor, we investigated long term storage. The prepared biosensors were stored under the same conditions at 4 °C for three weeks, and then the amperometric i-t curve current response was recorded. The current signal still remained at 90.4% compared with the initial value, manifesting the biosensor had good stability within three weeks.

The reproducibility of the biosensor was also evaluated by relative standard derivations (RSD) of inter-analysis and intra-analysis using the same concentration target DNA(100 pM, Fig. S6). The inter-assay RSD

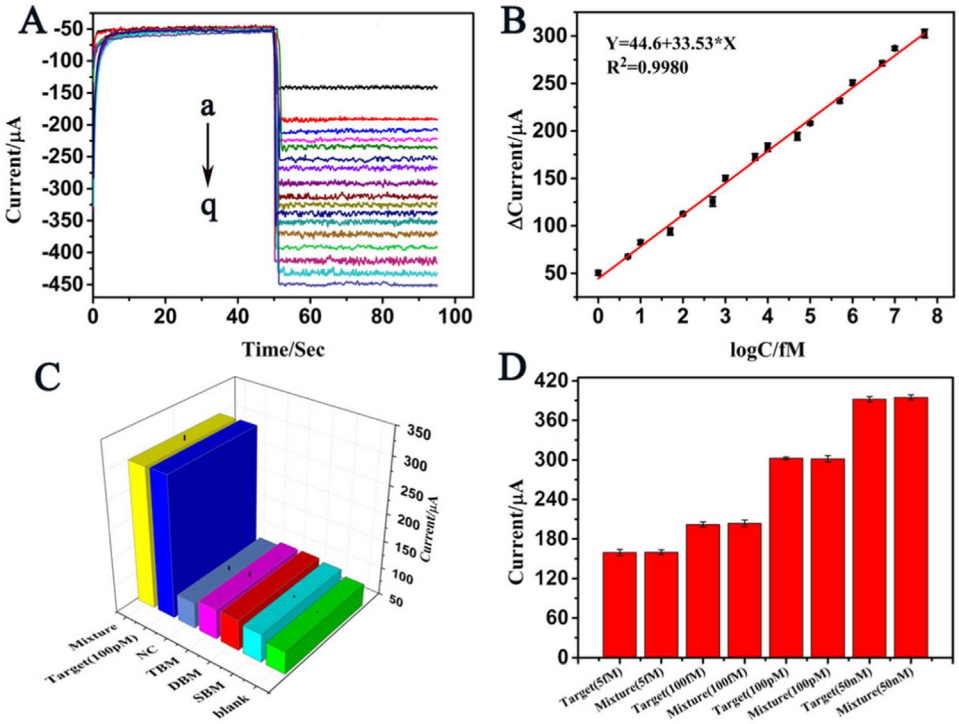

Fig. 3. The amperometric i-t curves of the proposed biosensor with different target DNA concentrations in 5 mL of PBS (pH 7.4) with the addition of H_2O_2 (1.4 mol L^{-1}): (A) a-q: 0–50 nM. (B) Calibration curve of the biosensor towards different concentrations of target DNA (a-q: 0–50 nM). The specificity of the biosensor was investigated with different ssDNA. (C): 100 pM target, mixture, blank control, 5 nM SBM, 5 nM DBM, 5 nM TBM and 5 nM NC. (D) 5 fM target, 100 fM target, 100 pM target, 50 nM target and relevant mixture, detailed parameter of various mixture is shown in Table S3. Error bars are the standard deviations across three repetitive experiments.

value was recorded as 1.3%, and the intra-assay RSD value was 1.27%. These results implied that the proposed biosensor has an acceptable reproducibility for the detection of target DNA.

3.9. Analytical application of biosensor

To evaluate the potential of the biosensor in clinical applications, four analyte concentrations (5 fM, 100 fM, 100 pM, 10 nM) were spiked into human serum samples, which were diluted 10-fold. First, target DNA was diluted by 10-fold-diluted serum samples. Then, we obtained the current of different concentrations target DNA by the amperometric i-t curve. Finally, the concentrations of target DNA were calculated by the standard curve method. The data are gathered in Table 1. The recovery response was recorded to fluctuate from 94.52% to 104.85% and the variation of RSD ranged from 1.24% to 3.48%, showing the potential applicability of this sensor in clinical applications.

Table 1
Recovery of *CYP2C19*2* gene in human serum samples.

Samples	Added	Found	Recovery (%)	RSD (%)
Sample-1	5 fM	5.08 fM	101.6	3.23
Sample-2	100 fM	104.85 fM	104.85	1.24
Sample-3	100 pM	98.10 pM	98.10	2.16
Sample-4	10 nM	9.45 nM	94.52	3.48

3.10. Detection of CYP2C19*2 gene in real sample

To further demonstrate the feasibility of the present biosensor for clinical application, the developed biosensors were incubated with 20 clinical serum samples at room temperature for 2 h. These above results were compared with those determined by sequencing. As shown in Table 2, thirteen serum specimens exhibited the negligible current responses (similar with or lower than that of blank and mismatch), implying no *CYP2C19*2* gene existed in these serum (negative results). Another seven groups of different serum specimens, the obviously increase in current responses were observed, indicating the existence of *CYP2C19*2* gene in these serum (positive result). In summary, the proposed biosensor method for *CYP2C19*2* gene detection was consistent with traditional method. The result indicated that the biosensor could effectively identify *CYP2C19*2* gene with high sensitivity and specificity.

Table 2
Assay results of *CYP2C19*2* gene in real serum sample that using the proposed method and reference method.

Specimen number	Pyrosequencing	The prepared biosensor	Current response (μA)[a]	ΔCurrent (μA)	Calculated concentration (fM)
S1-S13	–	–	–	–	–
S14	+	+	158.59	67.85	4.94
S15	+	+	153.6	62.86	3.50
S16	+	+	186.44	95.70	33.42
S17	+	+	145.28	54.54	1.98
S18	+	+	199.18	108.44	80.16
S19	+	+	158.68	67.94	4.91
S20	+	+	171.46	80.72	11.95

Notes: + represents the positive result of the *CYP2C19*2* type, — represents the negative result of the *CYP2C19*2* type.
[a] Calculated as a mean of three measurements.

4. Conclusion

In conclusion, a novel sandwich-type DNA biosensor was successfully developed for the detection of *CYP2C19*2* gene using c-C_{60}/CeO_2/PtNPs as a signal material. The developed biosensor exhibits broad linear ranges between current and the logarithm of *CYP2C19*2* gene concentrations (1 fM to 50 nM), low detection limit (0.33 fM), high specificity, good stability and excellent reproducibility. At the same time, the biosensor demonstrates resilience against endogenous interference in human serum, making it an ideal tool for clinical application. Furthermore, the biosensor will promote the greater use of c-C_{60}, CeO_2 and *Fe-MIL-88 MOFs* nanoparticles in the biosensor field. Therefore, the biosensor method can be used for the detection of trace amounts of DNA among copious background DNA, which is clinically meaningful. However the proposed biosensor cannot realize the determination of a multi-gene mutation. For this purpose, we will attempt to find potential applications in multiplexed assays and diagnostics by using different metal ion functionalized c-C_{60} as labels in our future work.

Acknowledgment

We are grateful for the financial support from the National Natural Science Foundation of China (No. 81370403), Chongqing Foundation and Advanced Research Project (No. CSTC2015jcyjBX0053), Chongqing Precision Medical Key Technology Research and Development and Demonstration Projects (cstc2016shms-ztzx0042), Chongqing Medical University Scientific Research Cultivating Fund (No. 201414) and Chongqing Graduate Scientific Research Innovation Project (No. CYS17159).

Appendix A. Supplementary material

Supplementary data associated with this article can be found in the online version at http://dx.doi.org/10.1016/j.bios.2017.11.014.

References

Angiolillo, D.J., Fernandez-Ortiz, A., Bernardo, E., Alfonso, F., Macaya, C., Bass, T.A., Costa, M.A., 2007. J. Am. Coll. Cardiol. 49, 1505–1516.
Bauer, T., Bouman, H.J., van Werkum, J.W., Ford, N.F., ten Berg, J.M., Taubert, D., 2011. BMJ 343, d4588.
Campo, G., Fileti, L., Valgimigli, M., Tebaldi, M., Cangiano, E., Cavazza, C., Marchesini, J., Ferrari, R., 2010. J. Thromb. Thrombolysis 30, 319–331.
Chen, Q., Yu, C., Gao, R., Gao, L., Li, Q., Yuan, G., He, J., 2016. Biosens. Bioelectron. 79, 364–370.
De Morais, S.M., Wilkinson, G.R., Blaisdell, J., Meyer, U.A., Nakamura, K., Goldstein, J.A., 1994. Mol. Pharmacol. 46, 594–598.
Deng, L., Chen, C., Zhu, C., Dong, S., Lu, H., 2014. Biosens. Bioelectron. 52, 324–329.
Dong, X.Y., Mi, X.N., Zhang, L., Liang, T.M., Xu, J.J., Chen, H.Y., 2012. Biosens. Bioelectron. 38, 337–341.
Hamm, C.W., Bassand, J.P., Agewall, S., Bax, J., Boersma, E., Bueno, H., Caso, P., Dudek, D., Gielen, S., Huber, K., Ohman, M., Petrie, M.C., Sonntag, F., Uva, M.S., Storey, R.F., Wijns, W., Zahger, D., Guidelines, E.S.C.C.F.P., 2011. Eur. Heart J. 32, 2999–3054.
Holmes, M.V., Perel, P., Shah, T., Hingorani, A.D., Casas, J.P., 2011. JAMA 306, 2704–2714.
Hu, L.M., Dai, D.P., Hu, G.X., Yang, J.F., Xu, R.A., Yang, L.P., Qian, J.C., Ge, R.S., Cai, J.P., 2012. Pharmacogenomics 13, 1571–1581.
Hulot, J.S., Bura, A., Villard, E., Azizi, M., Remones, V., Goyenvalle, C., Aiach, M., Lechat, P., Gaussem, P., 2006. Blood 108, 2244–2247.
Koukoula, M., Dotsikas, Y., Molou, E., Schulpis, K.H., Thodi, G., Chatzidaki, M., Triantafylli, O., Loukas, Y.L., 2017. J. Chromatogr. B 1047, 173–179.
Levine, G.N., Bates, E.R., Blankenship, J.C., Bailey, S.R., Bittl, J.A., Cercek, B., Chambers, C.E., Ellis, S.G., Guyton, R.A., Hollenberg, S.M., Khot, U.N., Lange, R.A., Mauri, L., Mehran, R., Moussa, I.D., Mukherjee, D., Nallamothu, B.K., Ting, H.H., American College of Cardiology, F., American Heart Association Task Force on Practice, G., Society for Cardiovascular, A., Interventions, 2013. Catheter Cardio Inte. 82, E266–E355.
Li, Q., Yu, C., Gao, R., Xia, C., Yuan, G., Li, Y., Zhao, Y., Chen, Q., He, J., 2016. Biosens. Bioelectron. 80, 674–681.
Li, Y., Yang, H., Zou, X., Xiong, L., Li, Z., Luo, J., Zhao, B., Liu, W., Du, X., 2014. Med. Sci. Monit. 20, 2213–2218.
Li, Y., Zhang, Y., Li, F., Feng, J., Li, M., Chen, L., Dong, Y., 2017. Biosens. Bioelectron. 92, 33–39.
Liu, N., Wang, Z., Ma, Z., 2014. Bioanalysis 6, 903–905.
Liu, Y.L., Zhao, X.J., Yang, X.X., Li, Y.F., 2013. Analyst 138, 4526–4531.
Lu, Q., Hu, H., Wu, Y., Chen, S., Yuan, D., Yuan, R., 2014. Biosens. Bioelectron. 60, 325–331.
Luo, H.R., Poland, R.E., Lin, K.M., Wan, Y.J., 2006. Clin. Pharmacol. Ther. 80, 33–40.
Mega, J.L., Simon, T., Collet, J.P., Anderson, J.L., Antman, E.M., Bliden, K., Cannon, C.P., Danchin, N., Giusti, B., Gurbel, P., Horne, B.D., Hulot, J.S., Kastrati, A., Montalescot, G., Neumann, F.J., Shen, L., Sibbing, D., Steg, P.G., Trenk, D., Wiviott, S.D., Sabatine, M.S., 2010. JAMA 304, 1821–1830.
Tang, X.F., Han, Y.L., Zhang, J.H., Wang, J., Yao, Y., He, C., Xu, B., Gao, Z., Qiao, S.B., Chen, J., Wu, Y., Chen, J.L., Gao, R.L., Yang, Y.J., Yuan, J.Q., 2016. Thromb. Res. 147, 108–114.
Ujjain, S.K., Das, A., Srivastava, G., Ahuja, P., Roy, M., Arya, A., Bhargava, K., Sethy, N., Singh, S.K., Sharma, R.K., Das, M., 2014. Biointerphases 9, 031011.
Wang, L., Ma, R., Jiang, L., Jia, L., Jia, W., Wang, H., 2017. Biosens. Bioelectron. 92, 390–395.
Wei, F., Lillehoj, P.B., Ho, C.M., 2010. Pediatr. Res. 67, 458–468.
Yu, B., Shu, X., Cong, H., Chen, X., Liu, H., Yuan, H., Chi, M., 2016. J. Chromatogr. A 1437, 226–233.
Yu, L.Q., Yan, X.P., 2013. Chem. Commun. 49, 2142–2144.
Zeng, D., Zhang, H., Zhu, D., Li, J., San, L., Wang, Z., Wang, C., Wang, Y., Wang, L., Zuo, X., Mi, X., 2015. Biosens. Bioelectron. 71, 434–438.
Zhang, J., Yuan, Y., biXie, S., Chai, Y., Yuan, R., 2014. Biosens. Bioelectron. 60, 224–230.
Zhang, Y., Hou, F., Tan, Y., 2012. Chem. Commun. 48, 2391–2393.